Shear banding and rheochaos in associative polymer networks

J. Sprakel,*[ab] E. Spruijt,[a] M. A. Cohen Stuart,[a] N. A. M. Besseling,[c] M. P. Lettinga[d] and J. van der Gucht[a]

Received 22nd February 2008, Accepted 14th April 2008
First published as an Advance Article on the web 20th June 2008
DOI: 10.1039/b803085e

We present experimental evidence of an instability in the shear flow of transient networks formed by telechelic associative polymers. Velocimetry experiments show the formation of shear bands, following a complex pattern upon increasing the overall shear rate. The chaotic nature of the stress response in transient flow is indicative of spatiotemporal fluctuations of the banded structure. This is supported by time-resolved velocimetry measurements.

1 Introduction

Physically crosslinked, micellar networks formed by telechelic associative polymers are popular model systems for studying the rheology of transient networks.[1–3] In dilute aqueous solutions these hydrophilic polymers, modified with a hydrophobic moiety at both chain ends, self-assemble into spherical, unconnected, micelles. The associative blocks (stickers) at both chain ends reside in the same micellar core, while the middle block (spacer) forms a loop in the corona. At higher concentrations (typically 0.1–1 wt%) bridging between the micelles leads to the formation of a sample-spanning network, where the spherical cores of the micelles form the junction points. This results in solutions that are characterised by a Maxwellian viscoelastic response with a single mechanical (zero-shear) relaxation time.[1] The reversible character of these systems can be tuned with the length and chemistry of the hydrophobic end blocks (stickers); the zero-shear relaxation time τ_0 can vary from tenths of milliseconds for small hydrocarbon tails to several hundreds of seconds for larger fluorocarbon tails.[4]

At low shear rates, solutions of associative polymers show Newtonian behaviour. When the reciprocal shear rate is of the order of the relaxation time or beyond, a rich variety of non-Newtonian responses is found. At moderate shear rates, shear thickening is observed, which is attributed to stretching of the polymer chains (bridges) due to the applied flow. At higher shear rates, strong shear thinning is found. This shear thinning is often explained as a decrease in the number of elastically active chains (bridges) in favour of the number of loops that do not contribute directly to the network.[5]

Berret and Séréro have shown that, in systems of fluorocarbon end-capped poly(ethylene oxide) with relaxation times many decades larger than those of the systems employed here, the first region of the shear thinning regime is characterised by an inhomogeneous flow, that appeared to resemble the planar fracture of solids.[6] Others have suggested that the rheology of similar transient networks, formed by adding telechelic polymers to microemulsions, shows the signs of shear banding,[5] but, so far, these conjectures have remained unsubstantiated. In this paper we present direct experimental evidence of such a shear banding transition in networks of telechelic associative polymers.

Shear-induced inhomogeneities are found in a variety of soft materials, such as linear aggregates of small surfactants (worm-like micelles),[7,8] linear supramolecular polymers,[9] rod-shaped colloids,[10] entangled polymers[11] and structured suspensions of spherical colloids.[12] The unstable flow in these systems leads to the formation of banded structures, either in the gradient direction (shear banding) or in the vorticity direction (vorticity banding). Three-dimensional inhomogeneities can also occur in certain cases.[13,14] Using model transient networks, consisting of physically crosslinked spherical micelles, we will argue that shear banding can be expected to be a common phenomenon in all networks with non-permanent crosslinks.

At rest, a phase transition driven by the entropy gain of bridge formation, can be found in some systems of telechelic polymers. Depending on the length of the stickers, the length of the spacer and the degree of functionalisation, solutions of telechelic polymers can demix into a viscous (network) phase rich in polymer and a dilute phase.[15] Computer simulations[16,17] and experiments[2,18] have shown that shear can induce anisotropy in transient micellar networks, as the bridges perpendicular to the flow direction will be disrupted more strongly than those in the flow direction. This is expected to lead to the formation of strings and/or sheets of micelles that are aligned in the flow direction and held together by bridges. Recent simulations show that shear banding can occur in systems of spherical particles with soft interactions,[19] which in essence is very similar to the systems used in this paper.

This paper focusses on the shear banding transition in networks of telechelic associative polymers, for which we present direct evidence using laser-Doppler velocimetry. In connection we will address the transient response of these systems in the shear banding regime. Stress relaxation mechanisms are observed on time scales many decades larger than the zero-shear relaxation time. In some cases the stress, rather than reaching a steady value, is found to show erratic fluctuations. This phenomenon,

[a]*Laboratory of Physical Chemistry and Colloid Science, Wageningen University, Dreijenplein 6, 6703 HB, Wageningen, The Netherlands. E-mail: joris.sprakel@wur.nl; Tel: +31-317-485595*
[b]*Dutch Polymer Institute (DPI), P.O. Box 902, 5600 AX Eindhoven, The Netherlands*
[c]*Section NanoStructured Materials, Department of Chemical Engineering, Delft University of Technology, Julianalaan 136, 2628 BL Delft, The Netherlands*
[d]*IFF, Institut Weiche Materie, Forschungszentrum Jülich, D-52425 Jülich, Germany*

often named rheochaos, is shown to be related to spatiotemporal fluctuations in the banded flow. Following Tanaka and Edwards[20] and Michel *et al.*,[5] we will explain the occurrence of the inhomogeneous flow as a direct result of the reduction of the relaxation time of stickers in the micellar cores, due to shear-induced stretching of the spacers. This approach leads to a simple constitutive equation specific to the microstructure of these systems that is experimentally evidenced based on results from superposition rheometry.

2 Experimental

2.1 Materials

The telechelic associative polymers that are studied here consist of a polyethylene oxide (PEO) spacer with a nominal M_W of 20 kg mol^{-1} and an octadecyl end group at both chain ends connected by urethane linkers. The PEO (Fluka) was dissolved in dry toluene (Sigma-Aldrich) and reacted with octadecyl isocyanate (Sigma-Aldrich) for 40 h at 80 °C in the presence of dibutyl tindilaurate (Sigma-Aldrich) as a catalyst. The modified polymers were isolated during three cycles of dissolution in toluene and precipitation in low-boiling petroleum-ether. Further purification comprised dissolution in demineralized water, double filtration over paper and 450 nm celluloseacetate membrane filters and removal of the solvent through freeze drying. It was found with ^{1}H-NMR that on average 1.9 alkyl tails (*i.e.* 95% conversion) were attached to each PEO chain. All samples were prepared by dissolving the polymer in demineralized water yielding optically transparent solutions. By studying the excimer formation of pyrene with fluorescence spectroscopy,[21] the critical micelle concentration for these polymers in water was found to be approximately 1×10^{-5} g L^{-1}.

2.2 Rheology

Rheological experiments were conducted on MCR300 and MCR301 rheometers (Paar Physica). Shear flow measurements were conducted in a Couette (concentric cylinder) geometry with an inner diameter of 16.66 mm and a gap width of 0.71 mm. Samples were left for at least 30 min after loading to equilibrate. Flow curves were recorded in various ways: (i) fast scans from low ($\dot{\gamma} = 0.1$ s^{-1}) to high shear rates ($\dot{\gamma} = 300$ s^{-1}), recorded with 25, 50 and 200 data points, with a measurement time of 1 s per point and (ii) slow scans from high ($\dot{\gamma} = 300$ s^{-1}) to low ($\dot{\gamma} = 1$ s^{-1}) shear rates, consisting of 50 data points in which the measured stress is averaged over 100 s. For the transient flow measurements, a fixed shear rate was imposed at $t = 0$, without any pre-shear treatment. Oscillatory measurements, to determine the viscoelastic properties of the transient networks, were conducted in a cone–plate set-up with a cone diameter of 50 mm, and tilt angle of 1°. Frequency sweeps were performed between 1 and 600 rad s^{-1}. These frequency sweeps were fitted with a single relaxation time Maxwell model,[1] to obtain the mechanical relaxation time τ and plateau modulus G. For the zero-shear properties, the strain was fixed at 5%, which was checked to be in the regime of linear response, giving access to the zero-shear relaxation time τ_0 and plateau modulus G_0. Standard rotational and oscillatory experiments were carried out under strain-controlled settings, which are realized with a feedback-loop in the rheometer hardware. Parallel superposition measurements, in which the oscillating frequency sweeps are superimposed on rotational shear flow, were carried out at a controlled stress of 10 Pa for the oscillatory motion and a varying controlled stress to accomplish the desired average shear rate.

2.3 Laser-Doppler velocimetry

Local velocity profiles of the shear flow of associative polymer networks were measured using heterodyne dynamic light scattering in combination with a differential laser-Doppler velocimeter. Note that these experiments are conducted with a different set-up to the rheometry measurements described above. The Couette cell had an inner diameter of 44 mm and a gap width of 2 mm. The optical part of the set-up consisted of a Kr laser beam (647 nm), split into two beams of equal intensity. These beams were focussed in a small volume of the gap of the transparent Couette cell. Scattered light was detected in the forward direction of the laser beam. The light scattered from each of the two beams has a different Doppler shift, and the resulting interference can be analysed to yield a local velocity of the sheared liquid. Wall positions were determined by measuring a velocity profile at a low shear rate, where the solutions are Newtonian and no slip or non-linear flow phenomena are expected. The size of the focal point of the two laser beams can be estimated from the diameter and divergence of the laser beam and the crossing angle at the focal point, resulting in a lower limit of about 100 μm. The temporal resolution is determined by the minimum time needed to measure an intensity autocorrelation function and was found to be of the order of 1 s, comparable to the limit found by Salmon *et al.*[22] In these experiments the inherent scattering of the micellar networks was used, hence no probe particles were added. Each velocity profile consists of 18 points across the gap, each of which has been averaged over 3 measurements of 10 s per data point.

3 Results and discussion

3.1 Steady-state rheology

The structure of solutions of telechelic associative polymers develops in 4 stages with increasing concentration, each with their own effect on the low shear viscosity (Fig. 1).[23] At low concentrations the chains exist as unimers (stage I), and the viscosity is approximately that of the solvent (here water). Above the critical micelle concentration (here found at 1×10^{-5} g L^{-1}) the chains associate into flowerlike micelles (stage II), and the viscosity increases slightly due to the added hydrodynamic volume of the micelles. Above a certain threshold the flowerlike micelles will form bridges, which leads to a sample-spanning transient network, with associative connections between the micellar cores (stage III). This is indicated by the sudden and steep increase in viscosity. The concentration threshold for network formation is found here at 6 g L^{-1}. All experiments are carried out well above this concentration. The dependence of the viscosity on the concentration in this regime is discussed by Annable *et al.*[1] At higher concentrations, entanglements of the flexible polymer spacer also become important (regime IV). We see this regime starting at roughly 20 g L^{-1}, which is around the overlap concentration for the unmodified analogue of the PEO

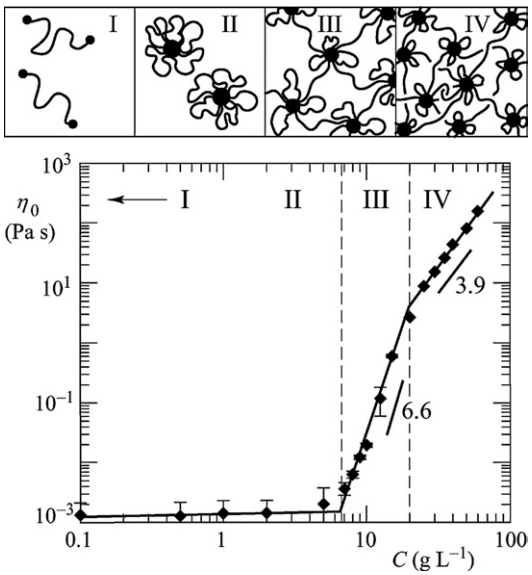

Fig. 1 Low shear viscosity of aqueous solutions of $C_{18}H_{37}$ end-capped PEO (M_W = 20 kg mol^{-1}) *versus* polymer concentration. 4 structural regimes are distinguished:[23] (I) unimers, (II) flowerlike micelles, (III) associative network of micelles connected through bridges (IV) associative network with entanglements. Drawn lines are power-law fits to the experimental data, exponents are indicated in the graph.

spacer used here. Similar observations as shown in Fig. 1 were made inref. 23.

The zero-shear viscoelasticity of these systems is known to be (close to) Maxwellian, thus characterised by a single mechanical zero-shear relaxation time τ_0 and plateau modulus G_0.[1] For the systems investigated, the relaxation times are between 2 and 7 milliseconds, and plateau moduli range from 10 Pa (10 g L^{-1}) up to 1×10^4 Pa (90 g L^{-1}) (Fig. 2).

The results just mentioned are all recorded well within the regime of linear response. In this paper we focus however on the non-linear rheology of these transient networks. With increasing overall shear rate, 4 different regimes can be distinguished (Fig. 3); at low shear rates the flow is Newtonian (regime A). At somewhat higher shear rates a modest shear thickening is found (regime B). This shear thickening has been studied in detail by others,[24,25] and is attributed to the stretching of the PEO middle

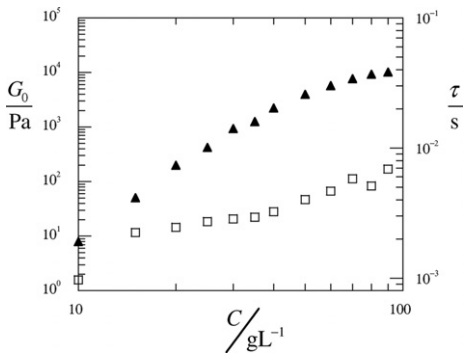

Fig. 2 Zero-shear relaxation times τ_0 (□) and plateau moduli G_0 (▲) as a function of polymer concentration, as obtained from fitting frequency sweeps to a single element Maxwell model.

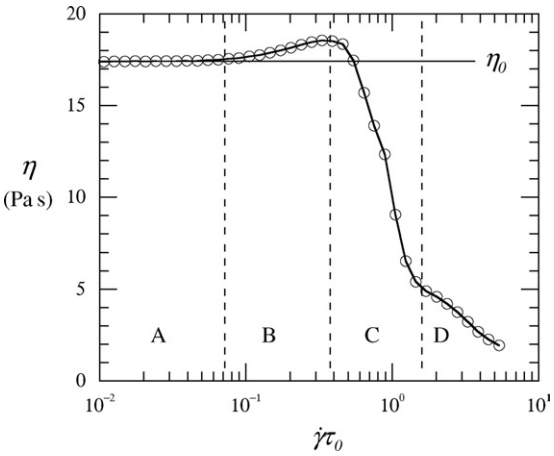

Fig. 3 Static viscosity *versus* imposed shear rate for a 30 g L^{-1} associative polymer solution, showing 4 different flow regimes with increasing shear rate: (A) Newtonian, (B) shear thickening, (C) and (D) shear thinning. Recorded at a scan rate of $\partial\ln(\dot{\gamma})/\partial t = 0.16$.

blocks, without decreasing the number of bridges between micelles. At higher shear rates the flow curves reveal shear thinning behaviour, which is the main focus of this paper. We will show that in the first part of the shear thinning, in regime C, the flow becomes inhomogeneous. In regime D, even though still shear thinning, the flow becomes homogeneous again.

In Fig. 4a we can see that the shape of the flow curve depends strongly on how it is obtained. Fast scans, from low to high shear rate, reveal a characteristic loop-like structure in the shear thinning regime, which becomes more pronounced if the scan is carried out faster, *i.e.* when $\partial\ln(\dot{\gamma})/\partial t$ is increased. This non-monotonic behaviour is an indication that the flow can become inhomogeneous. In classical shear banding theory, this loop, in analogy with a van der Waals loop for equilibrium phase transitions, is a metastable path which can lead to the flow decomposing into a banded structure with a high shear rate band at the inner rotating wall and a low shear rate band at the outer stationary wall. This would, in the ideal case, give a plateau in the stress through this metastable loop. The physical interpretation of this ideal plateau, with $\partial\ln\sigma/\partial\ln(\dot{\gamma}) = 0$ is similar to tie-lines in classical fluid coexistence, as it connects the two conditions (here shear rates) that coexist with each other. If the imposed shear rate is changed within this plateau, both the compositions and the shear rates in the bands stay constant, only the widths of the bands adjust (similar to a lever rule for classical fluid coexistence).

Two procedures for obtaining the flow curve have been attempted, see Section 3.2. The first is to start at high shear rates, and slowly decrease the shear rate into the Newtonian regime. This is shown as the thick drawn line in Fig. 4a. Another approach is to look at the transient (*i.e.* time-resolved) behaviour of the stress at a given imposed shear rate. It is expected that some time after switching on the shear flow, a stable stress value is obtained. The value of the stress at that point would correspond to the steady-state value. In our system however the stress does not reach a steady value, but continuously fluctuates after some initial relaxation. The magnitude of these fluctuations is indicated with the vertical bars in Fig. 4a.

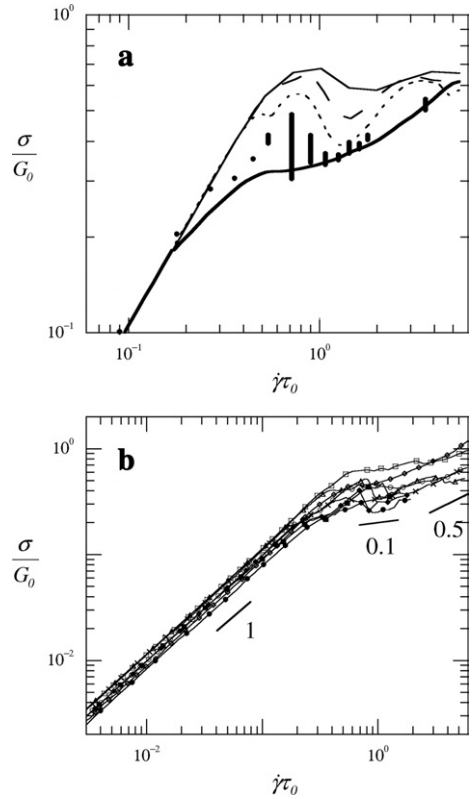

Fig. 4 (a) Flow curve ($c = 30$ g L^{-1}) obtained in various manners. Thin lines are scans from low to high shear rate with different scan speeds: $\partial\ln(\dot{\gamma})/\partial t = 0.32$ (solid), 0.16 (dashed) and 0.04 (dotted). Thick drawn line is a slow scan from high to low shear rate ($\partial\ln(\dot{\gamma})/\partial t = 0.01$). Vertical bars show the amplitude of the stress fluctuations, after the initial stress relaxation, during transient flow. (b) Dimensionless stress σ/G_0 *versus* dimensionless shear rate $\dot{\gamma}\tau_0$ as a function of telechelic polymer concentration c: ◇ 15 g L^{-1}, □ 20 g L^{-1}, ○ 25 g L^{-1}, × 30 g L^{-1}, △ 35 g L^{-1}, ◆ 40 g L^{-1}, ● 50 g L^{-1} and ■ 60 g L^{-1}.

We see that the transient points and the slow scan give approximately the same flow curve, in which the Newtonian regime is followed by strong shear thinning with $\partial\ln\sigma/\partial\ln(\dot{\gamma}) = 0.1$ (Fig. 4b), which we will show to be the sign of a shear banding transition.

In experiments on wormlike micelles, that also show a banding transition, a truly horizontal stress plateau is often found. Here we find a pseudo-plateau, with $\partial\ln\sigma/\partial\ln(\dot{\gamma}) = 0.1$. Two possible explanations for such a positive slope have been given. The first is that there is a coupling between concentration and flow, *i.e.* that the concentration of the two coexisting bands is not constant. Another explanation is found in the finite curvature of the Couette cell, leading to an inhomogeneous stress field across the gap.[26] The effect of cell curvature on the expected slope can be estimated with $\partial\ln\sigma/\partial\ln(\dot{\gamma}) \approx 2l/R_1$,[27] with l the gap width and R_1 the radius of the inner, rotating, cylinder. For the geometry in these experiments we find a predicted slope of 0.17. This suggests strongly that the finite slope of the shear banding plateau is caused by cell curvature effect. After this quasi-plateau, another shear thinning regime with $\partial\ln\sigma/\partial\ln(\dot{\gamma}) \approx 0.5$ is found, in which the flow becomes homogeneous again.

For Maxwellian fluids, which the systems under investigation here are, flow curves can be made to coincide by rescaling them with two parameters only: the zero-shear relaxation time τ_0 and the plateau modulus G_0. We see that this approach works for low shear rates (Fig. 4a), where the flow is Newtonian, but starts to deviate as soon as non-linear effects, such as the shear banding transition, come into play. This suggests that in the banded regime, secondary parameters become important such as the actual relaxation time(s) of the system rather than τ_0. We will discuss this in more detail in a following section. The minor deviations between the rescaled flow curves in the Newtonian regime might be explained by the experimental error associated with the determination of both G_0 and τ_0 and the fact that these parameters where measured in a different geometry (cone–plate) than the set-up used to determine the flow curves (Couette).

3.2 Stationary velocity profiles

Previously there has been speculation that the flow curves discussed in the previous section reveal signs of an inhomogeneous flow.[5] With laser-Doppler velocimetry we can show directly that this is indeed the case (Fig. 5a). At low shear rates, in the Newtonian regime, the velocity profiles are linear as expected for simple Couette flow. When we enter the shear thinning regime, for which the quasi-plateau is found in Fig. 4, we see that the steady-state velocity profiles are no longer linear, but show a banded structure, with bands of different shear rates coexisting with each other.

When the overall shear rate is further increased to the regime where $\partial\ln\sigma/\partial\ln(\dot{\gamma}) \approx 0.5$, the banded flow disappears. We note that the velocity profiles in this regime are approximately linear. Strong shear thinning leads to curved profiles in Couette flow,[27] but for the present geometry this occurs for values of $\partial\ln\sigma/\partial\ln(\dot{\gamma})$ significantly smaller than 0.5.

A closer view of the banded flow is given in Fig. 5c–f, in a sequence of increasing overall shear rates. The banding regime starts with a decomposition of the sample into two bands (5c and d), as expected in the classical picture. At somewhat higher shear there is a transition to an apparent 3 banded flow (5e). When the shear rate is further increased, the slowest band disappears and again two bands coexist with each other (5f). This process is also visualised in Fig. 6, where we see how the width of the three bands and their actual shear rates change throughout the shear banding regime. It is obvious that this complex progression of the banding is not in line with the classical picture, described in the previous section, where only the relative width of the bands changes with shear rate.

In Fig. 6a we can also see that no significant wall slip occurs at all shear rates, as the overall measured shear rate and the applied shear rate are consistent.

For transient networks of telechelic polymers with fluorocarbon stickers, Berret and Séréro have shown a solid-like fracture zone in the flow profile.[6] In these fluorocarbon-modified systems the zero-shear relaxation times are many decades larger (up to a factor of 1×10^6). It is conceivable that this fracture behaviour and our shear banding observations are of similar origin, but differ in manifestation due to this large difference in relaxation time.

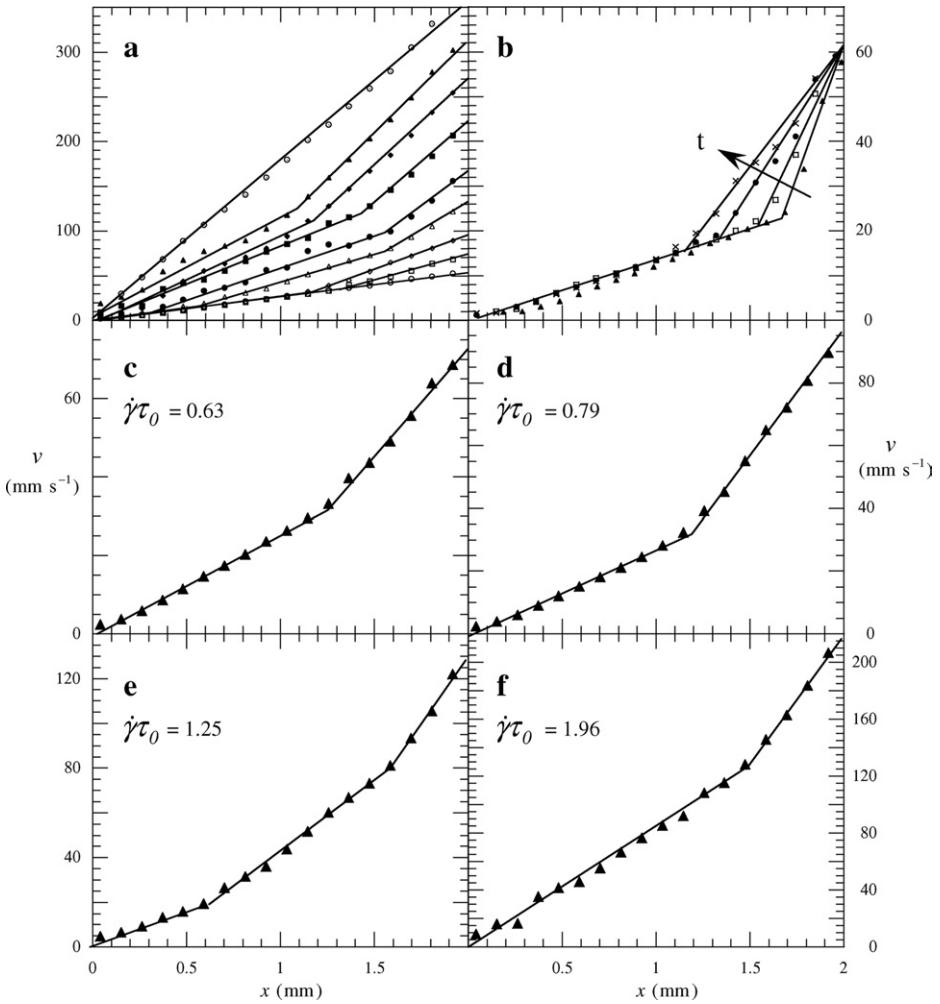

Fig. 5 Results from laser-Doppler velocimetry experiments for a 30 g L^{-1} solution of telechelic polymers. (a) An overview of the velocity profiles as a function of shear rate $\dot{\gamma} = 30$ ○, 41 □, 51 ◇, 81 △, 101 ●, 127 ■, 152 ◆, 177 ▲ and 203 s^{-1} ⊙. (b) Evolution of the velocity profile ($\dot{\gamma} = 30\ s^{-1}$) in time: 5 min ▲, 15 min □, 35 min ●, and 85 min × after start of the shear flow. (c)–(f) The same data as in (a), shown separately for clarity.

3.3 Simple constitutive equation

Following Tanaka and Edwards,[20,28] Michel *et al.*[5] developed a simple model to rationalise the non-monotonic flow curves found for transient networks of physically crosslinked microemulsions. This model is based on the reduction of the residence time of a hydrophobic sticker in a junction point due to flow-induced chain (spacer) stretching. In the following we describe a similar approach, that gives a microscopic view on why these transient networks show shear banding.

As stated in the introduction, the transient networks we study are formed from spherical micelles that are connected through polymeric bridges, *i.e.* the two stickers attached to a chain reside in different micellar cores. The chains that do not form a bridge are expected to form loops, *i.e.* both stickers are in the same micelle. At rest, the dynamics of the bridges can be described with a simple association–dissociation equilibrium:

$$\frac{\partial n_b}{\partial t} = k_a n_l - k_d n_b \tag{1}$$

where t is time, n_b the number of bridges, n_l the number of loops and $n = n_b + n_l$ is the total number of chains. The two reaction constants reflect the formation of bridges (k_a) and the dissociation of bridges (k_d). It is convenient to define an overall reaction constant as $K = k_a/k_d$ At steady-state the total number of bridges must be constant, $\partial n_b/\partial t = 0$, so:

$$n_b = \frac{Kn}{1+K} \tag{2}$$

Under shear deformation, the chains that form the bridges are continuously stretched, which gives rise to an elastic restoring force that pulls on the stickers. This force will enhance sticker dissociation. Here we assume an exponential relation between the lifetime of a bridge and the force:[28]

$$\tau = \tau_0 \exp\left(\frac{-f\delta}{k_B T}\right) \tag{3}$$

where τ_0 is the zero-shear residence time of the stickers, f the force acting on the chain ends associated with the stretching of the spacers and δ the length of the stickers. To calculate the force on the stickers, we assume that the chains are Gaussian, $f = r3k_BT/Na^2$, where r is the elongation of the chain and Na^2 is the square of the end-to-end distance of the undisturbed chain, with

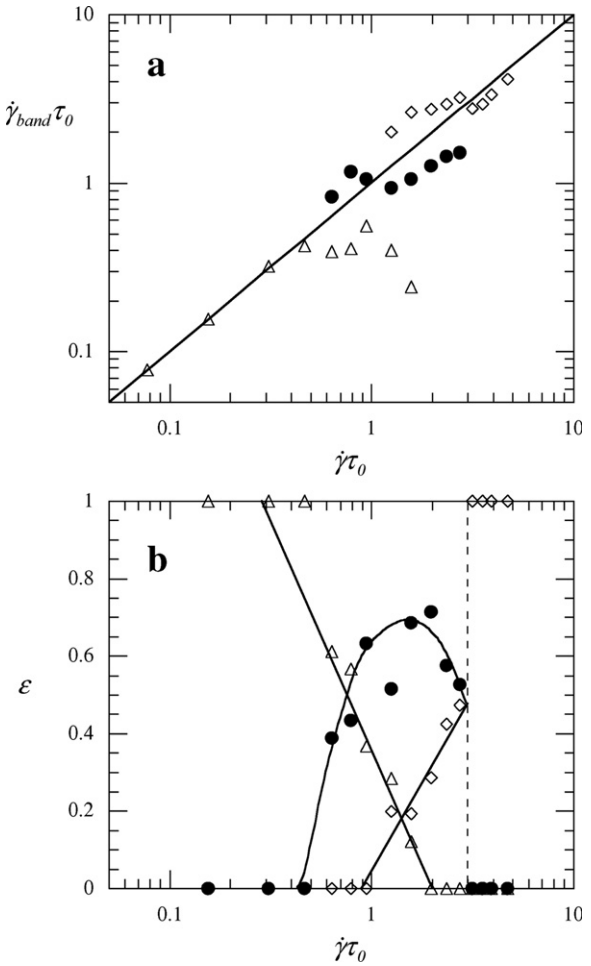

Fig. 6 (a) The average shear rate $\dot{\gamma}_{band}$ in the slow (△), intermediate (●) and the fast (◇) bands as a function of the applied shear rate $\dot{\gamma}$. The solid line indicates Newtonian flow. (b) The fraction of the gap (ε) occupied by the different shear bands as a function of the overall shear rate, showing the progression of the shear banded flow. Both are for a 30 g L^{-1} telechelic polymer solution. The disappearance of the shear bands is found to occur suddenly, as indicated by the dashed vertical line. Solid lines are drawn to guide the eye.

N the number of statistical segments and a their Kuhn length. In a time Δt at an imposed shear rate of $\dot{\gamma}$, the elongation is of the order of $r \approx \xi\Delta t\dot{\gamma}$, where $\xi = a\sqrt{N}$ is the end-to-end distance of the chain. During the lifetime of a bridge, the force then increases to approximately:

$$f \approx \frac{3k_BT}{\xi}\Delta t\dot{\gamma} \tag{4}$$

By combining eqn 3 and 4, we can write for the average residence time:

$$\langle\tau\rangle = \tau_0 \exp\left(-\frac{3\dot{\gamma}\langle\tau\rangle\delta}{\xi}\right) \tag{5}$$

The local stress, neglecting the contribution of the solvent, can be written as:

$$\sigma = \frac{f}{\xi^2}\frac{n_b}{n} \tag{6}$$

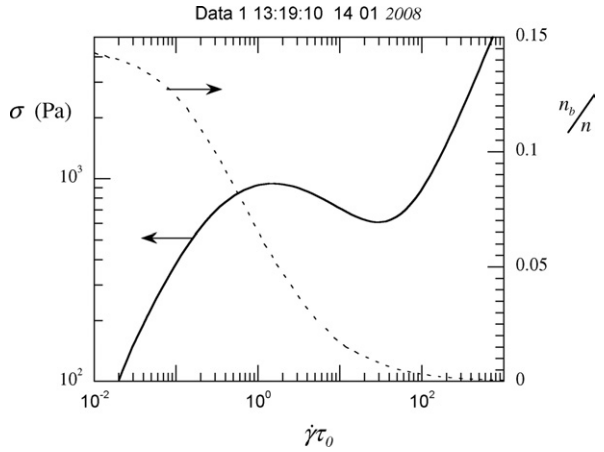

Fig. 7 The flow curve predicted by eqn 5 and 7, for $\tau_0 = 0.017$ s, $\delta = 1.8$ nm, $\xi = 5$ nm, $k_a = 10\ s^{-1}$ and $\eta_{eff} = 0.1$ Pa s. The dotted line indicates the corresponding change in the relative number of bridges n_b/n.

where n_b/n is the fraction of chains that is involved in a bridge. This gives:

$$\langle\sigma\rangle = \frac{3k_BT\dot{\gamma}\langle\tau\rangle}{\xi^3}\frac{k_a\langle\tau\rangle}{1+k_a\langle\tau\rangle} + \eta_{eff}\dot{\gamma} \tag{7}$$

where we have added the viscous contribution of the solvent $\eta_{eff}\dot{\gamma}$.

This constitutive equation predicts a non-monotonic flow curve (Fig. 7), which is indicative of a mechanical instability leading to shear banding. Although this approach does not give any specific details about banded flow, it does offer a qualitative explanation on a microstructural level. For these systems the inhomogeneous flow is the result of the increased breakdown rate of bridges in favour of loops (that are not significantly stressed by the flow), leading to a more than proportional decrease in the number of 'elastically active' chains (dotted line in Fig. 7).

3.4 Parallel superposition rheology

The model proposed in the previous section links the occurrence of inhomogeneous flow to the reduction of the 'relaxation' time of the stickers due to the applied shear flow. Using parallel superposition rheology, in which an oscillatory motion of the cone is superimposed on rotation, we can test this hypothesis.

In Fig. 8 three frequency sweeps performed at various imposed shear rates are given. As expected from the model, we see that the frequency where the storage and loss modulus intersect, which is equal to the reciprocal of the mechanical relaxation time τ, shifts to higher values with increasing shear rate. In other words, we indeed observe that the relaxation time decreases with increasing shear rate. For other types of associative polymer networks, similar observations have been made by Mewis *et al.*[29]

At low shear rates the relaxation times are of the same order as the zero-shear relaxation time τ_0, but at shear rates where we also find the onset of shear banding they start to decrease significantly (Fig. 9). In this figure the prediction by our model (eqn 5) is shown, for which we have entered realistic estimates for the input parameters, such as $\xi = 5$ nm, which is the radius of gyration of the PEO spacer for which $a = 0.7$ nm,[30] $\delta = 1.8$ nm which is the

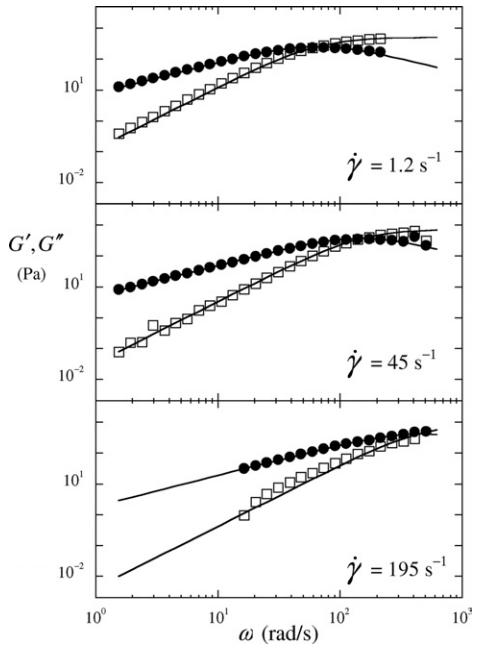

Fig. 8 Frequency sweeps for various superimposed shear rates, for a 25 g L^{-1} associative polymer solution. Experimentally obtained storage (G', □) and loss (G', ●) moduli and fits to a single Maxwell model (drawn lines).

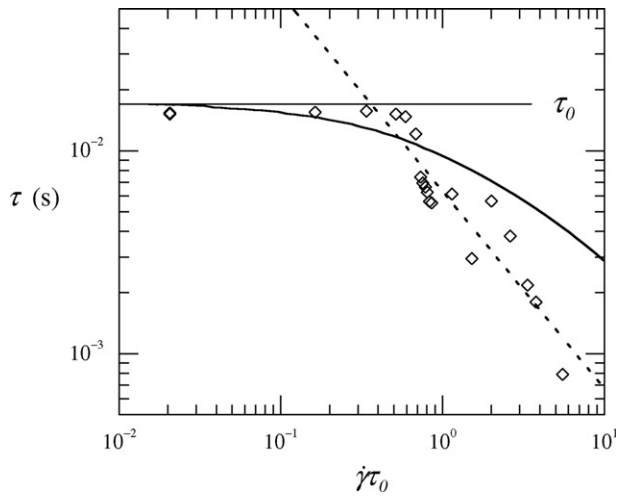

Fig. 9 Mechanical relaxation time *versus* superimposed shear rate, from parallel superposition measurements on a 25 g L^{-1} polymer solution. Horizontal drawn line indicates the value of the zero-shear relaxation time τ_0, curved drawn line is the decay of the relaxation time with shear rate as predicted by eqn 5 for $\delta = 1.8$ nm, $\xi = 5$ nm and $\tau_0 = 0.017$ s. Dotted line is a power-law fit to the decay of the relaxation time with $\tau \propto \dot{\gamma}^{-1}$.

contour length of a $C_{18}H_{37}$ alkyl tail and $\tau_0 = 0.017$ s as obtained from rheology measurements.

Qualitatively, the model predicts a similar behaviour as found in the experiments, which supports the hypothesis posed above, that indeed reduction of the relaxation time due to shear flow is responsible for the inhomogeneous flow. On a quantitative level the model is not very accurate and predicts a weaker decrease of the relaxation time $\tau(\dot{\gamma})$ than what is measured. We propose three explanations for this difference. First of all, the $\langle\tau\rangle$, that is obtained with eqn 5, is the average residence time of a sticker in a micellar junction point. This is of course not necessarily the same as the mechanical relaxation time obtained with rheometry. Secondly, the model only contains a few parameters and is intended for a qualitative explanation of the observed phenomena. It therefore might lack some important contributions, such as the effects of shear-induced structural changes in the network,[16] non-Gaussian chain stretching due to the flow[18] and the directionality in the breaking of bridges, which will be stronger in the direction perpendicular to the flow. Perhaps the most important explanation is that the predictions of eqn 5 assume the flow to remain homogeneous (*i.e.* follow the predicted, non-monotonic flow curve), whereas in the experiments the banding has most-likely already taken place, even in the cone–plate geometry used for these measurements.

3.5 Transient rheology

In a shear start-up experiment, a constant shear rate is imposed on the sample, starting at time $t = 0$, and the development of the stress, *i.e.* the transient stress response, is followed in time. For homogeneous flow it is expected that relaxation of the stress occurs on times scales of the order of the mechanical (Maxwell) relaxation time, here milliseconds. In the shear rate regime where shear banding is observed, in contrast, it can take tens of minutes for the stress to reach a steady plateau.

Various start-up stress responses are found when one goes through the shear banding regime. In some cases we find a classical stretched exponential decay (Fig. 10a), with a characteristic time of 2.7 s, *i.e.* $1000 \times \tau_0$, and a stretch exponent of 0.5. This type of stress decay, as studied in detail for wormlike micelles by Decruppe *et al.*,[31] is explained as a nucleation process followed by a one-dimensional growth of the fast band from the slow band. This is consistent with the evolution of the banded structure in transient flow, as shown in Fig. 5b. It starts with the formation of a thin band at the fast wall, which grows in width over approximately 90 min. Similar results are reported for systems of wormlike micelles.[7]

In the shear banding regime we find that after some initial relaxation of the stress, often no steady plateau is reached at all. The stress continuously fluctuates around a certain average (Fig. 10c–e and 11). These fluctuations are also indicated in the flow curves (Fig. 4a). A true steady-state flow does not exist in this regime.

This erratic behaviour in the stress, is now often called rheochaos.[13,14,31–33] However, the true chaotic nature of this type of fluctuation only becomes apparent after more careful considerations. First we can conclude that for most cases, the fluctuating stresses show a more or less Gaussian distribution (left insert Fig. 11), which is already an indication of a stochastic process. The power spectrum of this same data (right insert Fig. 11) reveals that there are no dominant frequencies, and that the power decays with roughly $1/f^{1.6}$, where f is the frequency. The qualification of true deterministic chaos however, implies that the power spectrum decays exponentially with the frequency,[32] which is not the case here.

In addition to the apparent chaotic or 'noisy' behaviour in Fig. 10c and 11, some conditions reveal intermittency, *i.e.* the

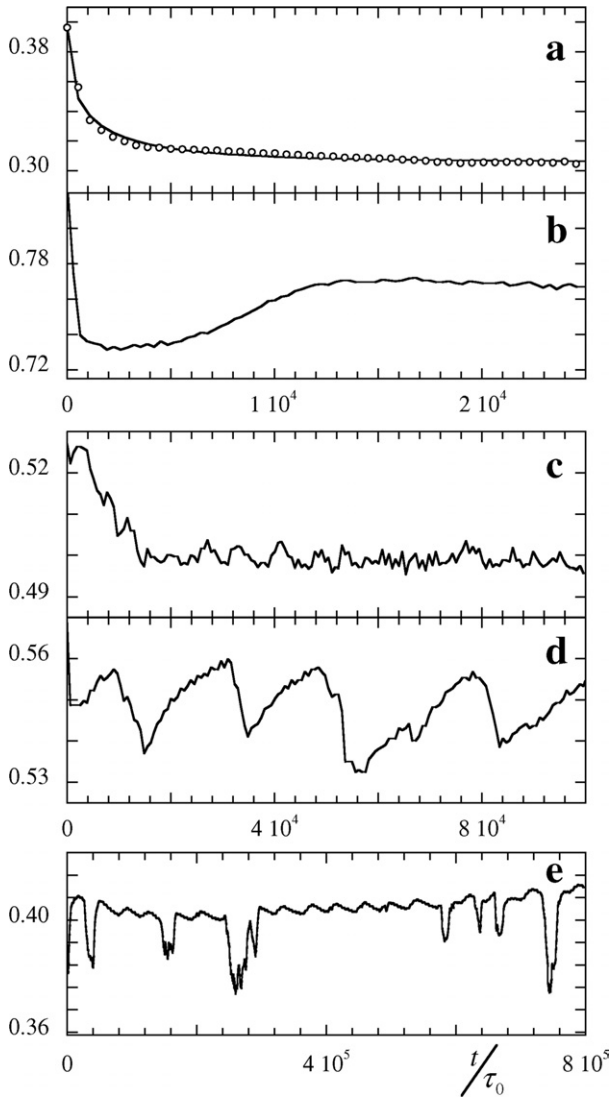

Fig. 10 Typical examples of transient stress responses in shear start-up experiments: (a) $c = 30$ g L^{-1} $\dot{\gamma}\tau_0 = 0.36$ (b) $c = 20$ g L^{-1} $\dot{\gamma}\tau_0 = 3.09$ (c) $c = 20$ g L^{-1} $\dot{\gamma}\tau_0 = 1.24$ (d) $c = 20$ g L^{-1} $\dot{\gamma}\tau_0 = 1.86$ (e) $c = 30$ g L^{-1} $\dot{\gamma}\tau_0 = 0.53$. In (a) the drawn line shows a fit to a stretched exponential decay, with a characteristic time of 2.7 s and a stretch factor of 0.5.

alternation of periodic and chaotic modes (Fig. 10d and e). Ganapathy and Sood suggest that rheochaos combined with intermittency can only occur when there is a coupling between banded flow and concentration.[32] Fielding and Olmsted have shown that such a coupling results in a non-horizontal stress plateau in the flow curve,[26] however curvature effects can also cause this same effect, as we discussed above. Nevertheless, we find both intermittency and a non-horizontal plateau, which might indicate that there is a coupling between flow and concentration in our system. The fact that it can take up to 90 min (Fig. 5b) for the steady banded state to form also suggests that some sort of transport (material and/or structure) is involved.

In attempts to quantify the concentration of polymers in the coexisting bands, using confocal microscopy on fluorescently stained samples, we did not find any measurable difference in

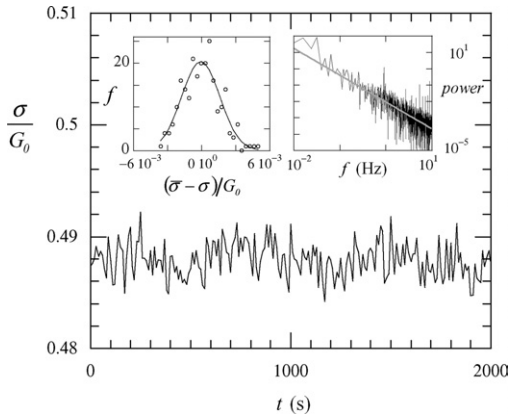

Fig. 11 Transient stress response ($c = 20$ g L^{-1}, $\dot{\gamma} = 70$ s^{-1}) revealing rheochaos. Insert left: distribution of the measured stresses, the drawn line is a Gaussian fit, right: power spectrum of the stress signal, the drawn line corresponds to $f^{-1.6}$.

polymer concentration between the shear bands. This suggests that concentration differences between the bands, if any, are small. We therefore might speculate that it is transport of structure that is time-limiting, rather than mass transport being the origin of the long relaxation times.

One explanation for rheochaos is spatiotemporal dynamics of the structure of the banded flow and the resulting fluctuations in the shape and position of the interface between the bands. Instead of the 'ideal' picture of 2 concentric bands, with an interface parallel to the wall, now more and more evidence is being presented, both experimentally[13,14] and theoretically,[33–35] of the occurrence a complex structure that changes in time.

Another cause for the fluctuating stresses might be continuous stick–slip transitions occurring at the rotating wall. It has been shown that this type of process gives a power spectrum of the stress signal that decays with approximately $1/f$,[36] not so different from what is found in Fig. 11.

To distinguish between these two possible causes of the rheochaos, we turn to the transient velocimetry experiments conducted at various positions in the gap of the Couette geometry (Fig. 12). It shows that in the centre of the gap, at and near the interface between the bands ($x = 1.2$ and 1.6 mm), there are significant fluctuations in the measured velocity, whereas the velocity is practically constant close to the stationary wall ($x = 0.4$ mm) or the rotating wall ($x = 1.9$ mm), with deviations of the order of the experimental accuracy of the technique.

These results suggest that the fluctuating stress is caused by the mechanical instability of the interface between the coexisting bands, rather than being the result of a stick–slip effect occurring at the wall. This is in line with our observation that no wall slip was observed in the velocity profiles. The fluctuations in velocity extend over macroscopic length scales ($\sim$1 mm). The explanation of rheochaos in terms of an interfacial instability is reviewed in detail by Fielding.[34]

3.6 Rheological diagram of states

With the observations of shear banding we can draw the diagram of states of the complex rheology of these types of associative networks (Fig. 13). It shows what type of behaviour is found as

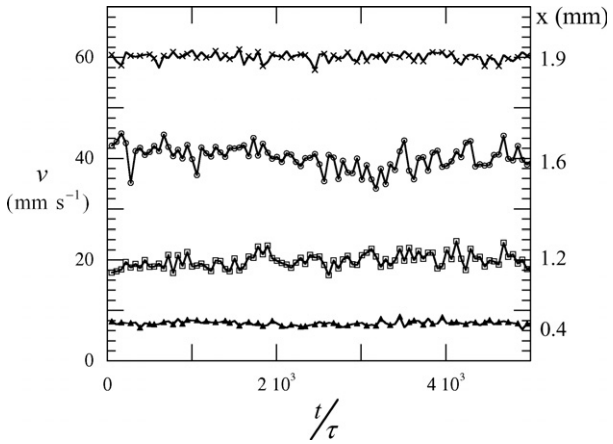

Fig. 12 Time evolution of the local velocity ($c = 30$ g L^{-1}, $\dot{\gamma} = 30$ s^{-1}). The corresponding positions in the Couette gap are denoted on the right side of the figure. Note that the absolute fluctuations near the moving and stationary wall (1.9 and 0.4 mm respectively) are much smaller than the fluctuations in the slow band (1.2 mm) and near the interface between the two bands (1.6 mm).

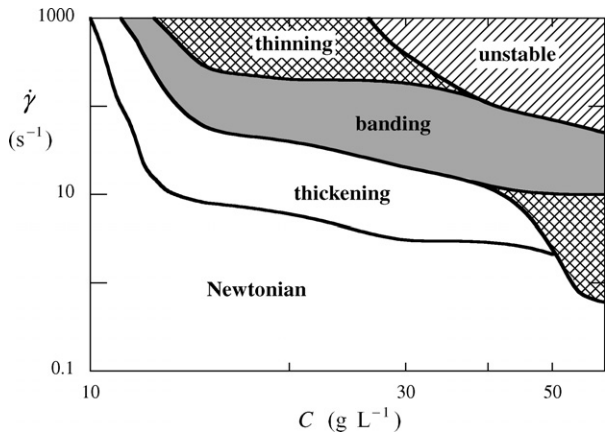

Fig. 13 Rheological diagram of states for a C_{18} end-capped PEO of 20 kg mol^{-1}, indicating the type of rheological behaviour as a function of concentration and imposed shear rate, as determined experimentally.

a function of both polymer concentration and imposed shear rate. It had already been established that the Newtonian regime at low shear rates is followed by shear thickening, and subsequently changes into strong shear thinning. We have now shown directly, that the onset of the shear thinning regime is characterised by a shear banding transition. As we could see in Fig. 6, the upper and lower shear rate where shear banding occurs was experimentally accessible for this system. When we exit the shear banding regime by increasing the shear rate beyond this upper limit, the flow becomes homogeneous again, yet is still shear thinning (see also Fig. 4).

However, at even higher shear rates the flow becomes macroscopically unstable and is accompanied by the sample being expelled from the measurement geometry. Visual inspection of the set-up under these conditions (Fig. 14), reveals that the liquid climbs up the rotating axis of the rheometer. This rod-climbing, or Weissenberg, effect is often attributed to the

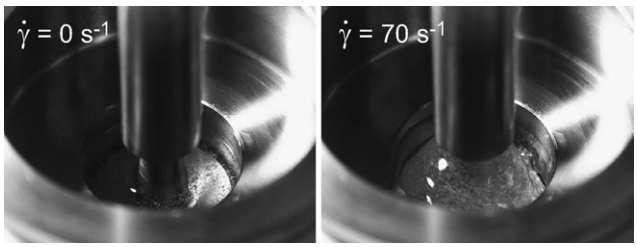

Fig. 14 Photograph of a telechelic polymer solution in the Couette geometry at rest (left) and during shear (right), showing the Weissenberg effect.

development of large normal stress differences. This behaviour is indicated in Fig. 13 as *unstable*.

Other instabilities can be excluded here.[37] The inertial Couette–Taylor instability occurs at Taylor numbers larger than the critical value of 1712. This dimensionless Taylor number is defined as:

$$Ta = \frac{l}{R_1} Re^2 = \frac{\rho^2 \dot{\gamma}^2 l^5}{\eta^2 R_1} \tag{8}$$

where Re is the Reynolds number, R_1 the radius of the inner cylinder (8.33 mm), l the gap width (0.71 mm) and ρ the density of the liquid ($\approx$ 1000 kg m^{-3}). For a 50 g L^{-1} solution of associative polymers, we find the instability to occur at $\dot{\gamma} = 60$ s^{-1} at a viscosity of 21 Pa s. This gives $Ta = 4 \times 10^{-8}$, hence inertial effects are completely negligible.

The purely elastic instability described for other shear banding systems,[37] can also be excluded. It is expected to occur at a critical shear rate equal to:

$$\dot{\gamma}^c = \frac{5.9}{\tau_0} \left(\frac{l}{R_2} \right)^{-\frac{1}{2}} \tag{9}$$

where R_2 is the radius of the outer cylinder (9.04 mm). For the same sample (50 g L^{-1}), with a zero-shear relaxation time of 25 ms, $\dot{\gamma}^c = 842$ s^{-1}. The instability we observe appears at 60 s^{-1} and is therefore expected to be neither inertial nor elastic in origin, rather caused by normal stress differences, leading to a Weissenberg effect.[38]

4 Conclusions

In this work we have shown direct evidence for a shear banding transition in transient networks of associative polymers under shear flow. Our results indicate that the banded flow does not obey the 'ideal' picture of shear banding. Deviations are found in the non-horizontal plateau, chaotic transient stress response and the unusual progression of the banded structure, as illustrated in Fig. 6. A possible explanation can be found in the fact that there seems to be a time-limiting transport process, most likely being the transport of structure to form the final bands. We have also observed that the structure of the banded flow is strongly non-stationary both in time and in space, with structure fluctuations extending over macroscopic dimensions. As a result, no steady stress is reached in transient flow; the stress continuously fluctuates in a chaotic or intermittent manner.

The explanation of the observed banding transition, found in the facilitation of breaking elastically active junctions in the network due to the applied shear, has been verified experimentally using parallel superposition rheometry. We pose that shear banding is, in principle, the direct result of the influence of shear forces on the lifetime of junction points in reversible networks, and can therefore be expected to occur in (almost) all transient networks.

With the direct evidence for complex shear banding in these model transient networks, new opportunities for investigating this phenomenon arise. With these systems the internal interactions, and hence the tendency for phase separation at rest, can be tuned by changing the molecular architecture, *i.e.* the length and chemistry of the hydrophobic stickers or soluble middle block. The importance of hydrodynamic and/or thermodynamic contributions to the observed flow-induced transition might be investigated systematically in this way.[39] Changing the end blocks also drastically alters the mechanical relaxation time, which depends exponentially on the length of the stickers. This flexibility in designing these molecules, and their well-defined and understood structure, makes these model networks interesting alternatives to wormlike micelles for studying shear-induced transitions.

Acknowledgements

We gratefully acknowledge Dr Hartmut Kriegs for technical assistance during the velocimetry experiments. The work of J. Sprakel forms part of the research programme of the Dutch Polymer Institute (DPI), project #564.

References

1 T. Annable, R. Buscall, R. Ettelaie and D. Whittlestone, *J. Rheol.*, 1993, **37**, 695–726.
2 K. Tam, R. Jenkins, M. Winnik and D. Bassett, *Macromolecules*, 1998, **31**, 4149–4159.
3 J. Berret, Y. Séréro, B. Winkelman, D. Calvet, A. Collet and M. Viguier, *J. Rheol.*, 2001, **45**, 477–492.
4 J. Berret, D. Calvet, A. Collet and M. Viguier, *Curr. Opin. Colloid Interface Sci.*, 2003, **8**, 296–306.
5 E. Michel, J. Appell, F. Molino, J. Kieffer and G. Porte, *J. Rheol.*, 2001, **45**, 1465–1477.
6 J. Berret and Y. Séréro, *Phys. Rev. Lett.*, 2001, **87**, 048303.
7 E. Miller and J. P. Rothstein, *J. Non-Newtononian Fluid Mech.*, 2007, **143**, 22–37.
8 E. Fischer and P. T. Callaghan, *Phys. Rev. E*, 2001, **64**, 011501.
9 J. van der Gucht, M. Lemmers, W. Knoben, N. A. M. Besseling and M. P. Lettinga, *Phys. Rev. Lett.*, 2006, **97**, 108301.
10 K. G. Kang, M. P. Lettinga, Z. Dogic and J. K. G. Dhont, *Phys. Rev. E*, 2006, **74**, 026307.
11 P. Tapadia, S. Ravindranath and S. Q. Wang, *Phys. Rev. Lett.*, 2006, **96**, 196001.
12 A. Imhof, A. van Blaaderen and J. K. G. Dhont, *Langmuir*, 1994, **10**, 3477–3484.
13 M. R. Lopez-Gonzalez, W. M. Holmes and P. T. Callaghan, *Soft Matter*, 2006, **2**, 855–869.
14 L. Becu, D. Anache, S. Manneville and A. Colin, *Phys. Rev. E*, 2007, **76**, 011503.
15 Q. Pham, W. Russel, J. Thibeault and W. Lau, *Macromolecules*, 1999, **32**, 2996–3005.
16 P. Khalatur, A. Khokhlov and D. Mologin, *J. Chem. Phys.*, 1998, **109**, 9602–9613.
17 P. Khalatur, A. Khokhlov and D. Mologin, *J. Chem. Phys.*, 1998, **109**, 9614–9622.
18 L. Pellens, J. Vermant and J. Mewis, *Macromolecules*, 2005, **38**, 1911–1918.
19 A. van den Noort and W. J. Briels, *Macromol. Theory Simul.*, 2007, **16**, 742–754.
20 F. Tanaka and S. Edwards, *Macromolecules*, 1992, **25**, 1516–1523.
21 H. Siu and J. Duhamel, *Macromolecules*, 2005, **38**, 7184–7186.
22 J. Salmon, L. Bécu, S. Manneville and A. Colin, *Eur. Phys. J. E*, 2003, **10**, 109–221.
23 E. Regalado, J. Selb and F. Candau, *Macromolecules*, 1999, **32**, 8580–8588.
24 G. Marrucci, S. Bhargava and S. Cooper, *Macromolecules*, 1993, **26**, 6483–6488.
25 S. Ma and S. Cooper, *Macromolecules*, 2001, **34**, 3294–3301.
26 S. M. Fielding and P. D. Olmsted, *Eur. Phys. J. E*, 2003, **11**, 65–83.
27 J. Salmon, A. Colin, S. Manneville and F. Molino, *Phys. Rev. Lett.*, 2003, **90**, 228303.
28 F. Tanaka and S. Edwards, *J. Non-Newtonian Fluid Mech.*, 1992, **43**, 289–309.
29 J. Mewis, B. Kaffashi, J. Vermant and R. Butera, *Macromolecules*, 2001, **34**, 1376–1383.
30 S. K. Pattanayek and V. A. Juvekar, *Macromolecules*, 2002, **35**, 9574–9585.
31 J. Decruppe, S. Lerouge and J. Berret, *Phys. Rev. E*, 2001, **63**, 022501.
32 R. Ganapathy and A. Sood, *Phys. Rev. Lett.*, 2006, **96**, 108301.
33 A. Aradian and M. E. Cates, *Phys. Rev. E*, 2006, **73**, 041508.
34 S. M. Fielding, *Soft Matter*, 2007, **3**, 1262–1279.
35 S. Fielding and P. Olmsted, *Phys. Rev. Lett.*, 2006, **96**, 104502.
36 H. Feder and J. Feder, *Phys. Rev. Lett.*, 1991, **66**, 2669–2672.
37 S. Manneville, A. Colin, G. Waton and F. Schosseler, *Phys. Rev. E*, 2007, **75**, 061502.
38 P. Kundu, *Trans. Soc. Rheol.*, 1973, **17**, 343–349.
39 J. Dhont, *Phys. Rev. E*, 1999, **60**, 4534–4544.